Fachtagung "Experimentelle Strömungsmechanik"
3. - 5. September 2024, Berlin

Macroscopic Fuel Spray Characteristics at Sub/Transcritical Injection Conditions

Min Son, Lars Zigan, Michael Pfitzner, Tobias Sander
Institute of Thermodynamics, Universität der Bundeswehr München, Neubiberg, Germany

Keywords: Transcritical Spray, Phase Transition, Optical Diagnostics

Abstract

This study investigates the phase change phenomena of cyclopentane fuel sprays under subcritical and transcritical conditions in a high-pressure, high-temperature chamber using optical diagnostics. Three optical techniques were employed to analyze the spray characteristics: shadowgraphy (SH), Mie scattering (MS), and infrared radiation (IR) measurements. SH and MS techniques revealed how quickly the phase transition from liquid to gas or supercritical fluid happens. MS results presented step-like transition behavior for subcritical sprays and smooth changes for transcritical sprays. IR measurements showed bimodal radial signal intensity distributions of transcritical sprays at downstream the liquid phase. Large signals at the spray boundary may indicate the onset of supercritical conditions. The findings in this study will support the development of computational models for phase transitions in fuel sprays. The results offer valuable data for optimizing combustion efficiency and reducing emissions in advanced combustion systems.

Introduction

Fuel injection into a high-pressure, hot gas environment is common in various combustion devices such as internal combustion engines, gas turbine engines, and liquid rocket engines (Lin 2011, Liu et al. 2017, Ma et al. 2014). The combustion chamber pressure often exceeds the critical point, leading to phase changes and transcritical behavior in the fuel spray (Wensing et al. 2016). The phase change at the spray boundary, where the fuel mixes with the ambient gas, is complex and influenced by the mixture ratio, changing the mixture's critical point and resulting in phase separation at the spray interface (Chehroudi et al. 2002, Traxinger et al. 2019). This phenomenon has been proven to be significant even in liquid rocket combustion, previously thought to involve only simple supercritical mixing (Oschwald et al. 2006). To improve combustion efficiency and reduce emissions in combustion engines (Ahern et al. 2001), it is important to understand the phase transition in fuel sprays at transcritical conditions, which means subcritical injection into a supercritical environment (Bellan 2020).

This study aims to investigate the phase change phenomena of fuel sprays under subcritical and transcritical conditions. The phase-change characteristics of cyclopentane fuel sprays were observed in a high-pressure, high-temperature spray chamber using three optical diagnostics: focused shadowgraphy, Mie scattering, and infrared radiation measurements. This paper first describes the experimental setup for the three optical diagnostics and then discusses the results obtained from spray images to explain differences between subcritical

GALA e.V., Karlsruhe, Germany, ISBN 978-3-9816764-4-0

and transcritical sprays. The experimental results will support computational and molecular dynamic simulations within the interdisciplinary dtec.bw project “MaST – Makro/Mikro-Simulation des Phasenzerfalls im Transkritischen Bereich” (Neumann et al. 2022).

Experimental Setup and Methods

Fuel spray was injected into a high-pressure chamber known as the OptiVeP, capable of operating from 30 kPa to 10 MPa and up to 1000 K (Riess et al. 2018). The chamber has one sapphire window and four quartz windows (125-mm diameter), with an injector flange at the bottom. A single-hole research injector with a nozzle diameter of 0.2 mm was used. Cyclopentane (C_5H_{10}), pressurized with a dual pneumatic high-pressure pump, was temperature controlled via a thermostat-heated injector flange. The chamber was pressurized with nitrogen to prevent chemical reactions, allowing mixing between cyclopentane and nitrogen to occur.

Three optical diagnostics were used: shadowgraphy (SH), Mie scattering (MS), and infrared radiation (IR) measurements. SH captures spatial derivatives of rays distorted by differences in refractive index caused by changes in density, temperature, and species, while MS detects droplets through elastic scattering. Combining SH and MS methods identifies liquid and non-liquid regions. The IR technique measures thermal radiation from the fuel jet, highlighting differences between subcritical and transcritical jets.

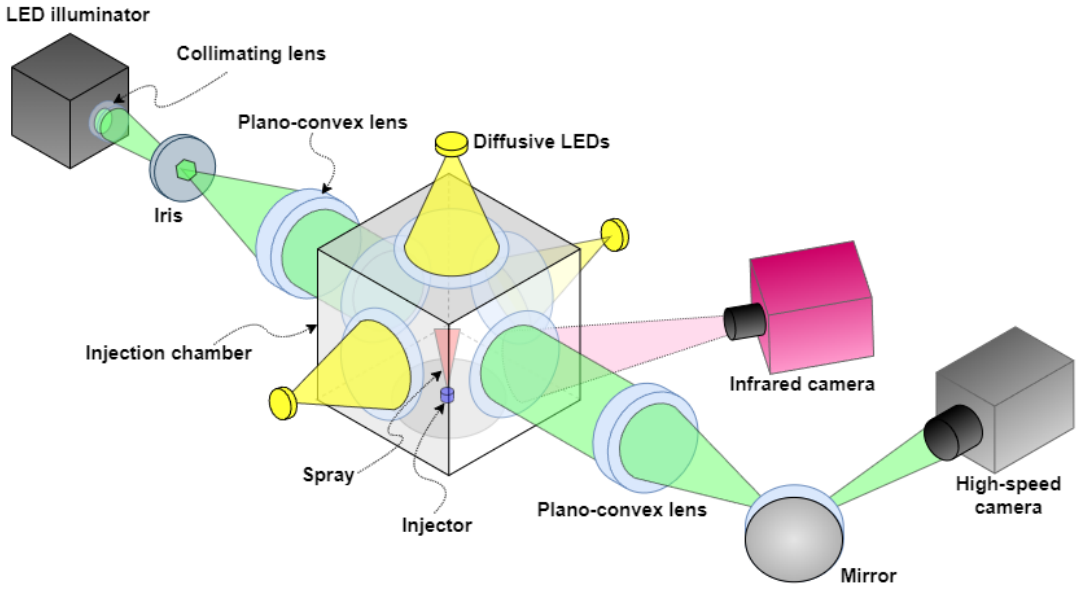

Fig. 1: Experimental setup for three optical diagnostics

Two cameras and two light sources were used for these diagnostics as shown in Fig. 1. For SH, a green LED (HARDsoft IL-105G) illuminated the spray from the back, which was captured as shadows by a high-speed camera (Photron Fastcam SA-Z) at 40,000 fps and 1 µs exposure. For MS, three diffused LED lights illuminated the spray from the side, using the same camera at 5 µs exposure. Simultaneous MS and SH measurements were not possible, so light sources were alternated. IR measurements were conducted independently with an IR camera (Telops M2K) at a tilted angle to avoid reflections of the cooled sensor from the sapphire window, using a frame rate of 4,000 fps, an exposure time of 40 µs, and a band-pass filter (2.9 µm - 3.5 µm). The resolutions were 93.4 µm/px for the high-speed camera and 425.5 µm/px for the IR camera.

GALA e.V., Karlsruhe, Germany, ISBN 978-3-9816764-4-0

Table 1: Experimental conditions for subcritical and transcritical sprays

Case	P_c [bar]	T_c [K]	P_{inj} [bar]	T_{inj} [K]	$P_{r,c}$	$T_{r,c}$
1	40	465	82	293	0.88	0.91
2	40	564	83	293	0.88	1.1
3	55	564	98	293	1.2	1.1
4	55	563	99	373	1.2	1.1

Four cases were defined to compare spray characteristics under different conditions, as listed in Table 1. Cases 1 and 2 were subcritical injections, while cases 3 and 4 were transcritical. The chamber pressure and temperature (P_c and T_c) and injection pressure and temperature (P_{inj} and T_{inj}) were measured with uncertainties less than 1%, except for injection temperature, which has an uncertainty of less than 0.1 K (JCGM 2008). The reduced pressures and temperatures ($P_{r,c}$ and $T_{r,c}$) were based on cyclopentane's critical point, calculated by CoolProp (Bell et al. 2014).

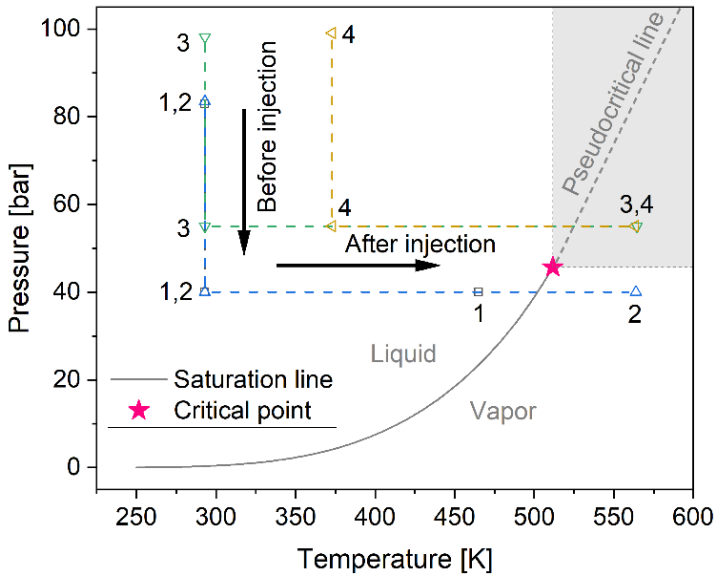

Fig. 2: Experimental conditions on a cyclopentane phase diagram

Figure 2 shows the experimental conditions on a cyclopentane phase diagram, with points indicating injection and chamber conditions. Dashed lines illustrate intuitive changes in fuel properties from the injector into the chamber. The injection pressure matches the chamber pressure before the jet enters the chamber, and its temperature changes from subcritical to supercritical as it mixes with the ambient gas.

Results and discussion

The injector operated for 3 ms, and the sprays after 2.0 ms after start of injection is regarded as in a steady state near the injector tip. Hence, the spray angle and penetration depth were quantitatively compared at 3 ms after start of injection. The spray angle, defined as the full cone angle measured near the injector, and the spray penetration depth, defined as the furthest spray tip from the injector, were measured for each spray snapshot and ensemble-averaged for 32 shots through the postprocessing procedure.

GALA e.V., Karlsruhe, Germany, ISBN 978-3-9816764-4-0

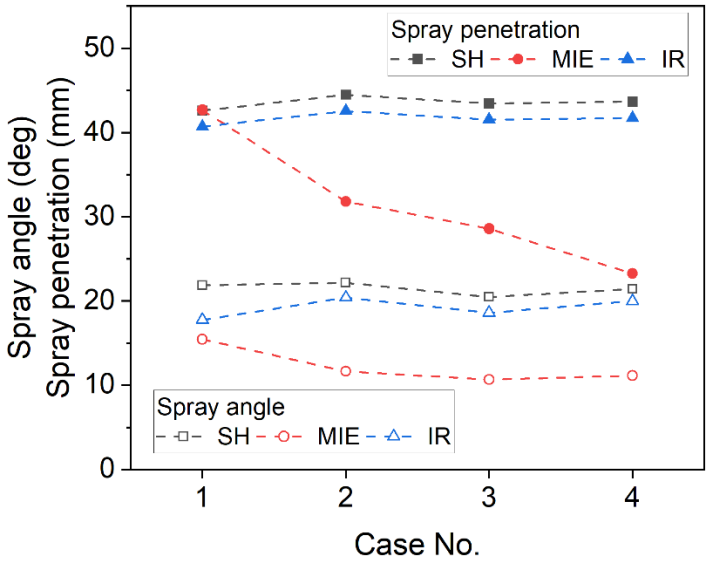

Fig. 3: Comparison of spray angles and penetration depths at 3 ms after start of injection

As shown in Fig. 3, the results from shadowgraphy and IR measurements show a similar trend in spray angles and penetration depth. However, the IR measurement underestimates the spray penetration depth and angle compared to shadowgraphy. This underestimation could be due to the sensitivity of the IR camera to temperature and its low temporal and spatial resolutions. Meanwhile, the MS results exhibit a different trend, with the liquid spray penetration depth being highly affected by changes in the chamber conditions. Specifically, when the chamber temperature increases, the penetration depth reduces drastically, and the injection temperature also has a noticeable effect. Similarly, the spray angle from the MS technique is strongly influenced by the chamber temperature.

To compare images from the three methods, 32 sets of spray images were averaged at each frame, as shown in Figures 4, 5, and 6. All images were normalized to their respective maximum so that the intensity range from 0 to 1, while keeping the same thresholds for each method. From the shadowgraphy images, the region with the lowest intensity (highest optical density) can be assumed to be a dense liquid core, as the dense liquid phase blocks the backlight, while the light gaseous phase allows light to pass through, as seen in Figure 4. This dense core is more clearly visible in the MS images, as shown in Figure 5, since MS only occurs e.g. with a liquid structure in a gas (Wensing et al. 2016). Hence, the MS signal directly represents the existence of the liquid core. However, it should be noted that the liquid core consists of small droplets rather than a single liquid column, since the injection Reynolds number ($> 5.5\times10^4$) and Weber number ($> 9.4\times10^4$) are already high enough to induce atomization breakup from the injector nozzle (Reitz und Bracco 1986). The strong MS signals match well with the low-intensity region of the shadowgraphy images. When the chamber temperature increases from 465 K (Case 1) to 564 K (Case 2), the liquid core is dramatically shortened, as seen in Figs. 5(a) and (b). Additionally, an increase in injection temperature partially affects the length of the liquid core, as shown in Figs. 5(c) and (d).

IR images are subtracted by background radiation to obtain the radiation from sprays, as shown in Fig. 6. The chamber temperature in Case 2 is 100 K higher than in Case 1, which can explain the overall differences in intensity between the two cases. Strong IR signals are observed in the region of the dense spray core in Cases 2-4, which corresponds to the liquid phase core observed from other methods. There are two potential explanations for this.

GALA e.V., Karlsruhe, Germany, ISBN 978-3-9816764-4-0

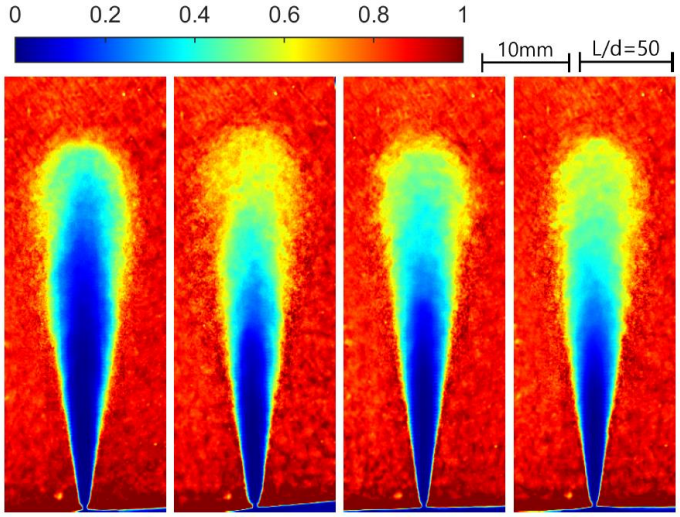

(a) Case 1 (b) Case 2 (c) Case 3 (d) Case 4

Fig. 4: Averaged SH images at 3 ms after start of injection (false-colored)

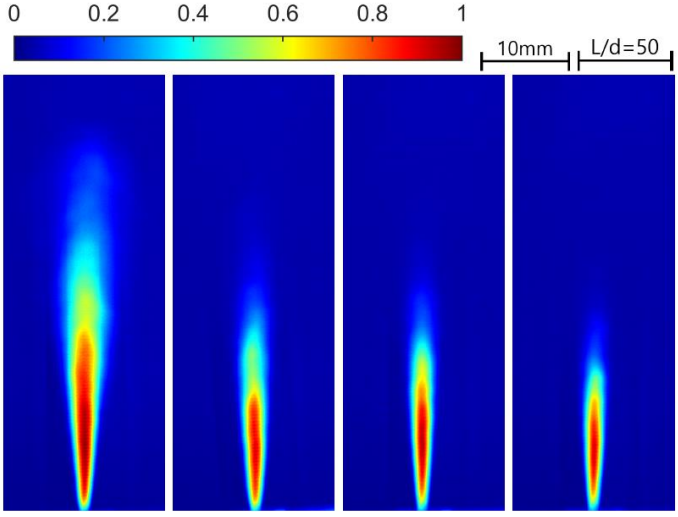

(a) Case 1 (b) Case 2 (c) Case 3 (d) Case 4

Fig. 5: Averaged MS images at 3 ms after start of injection (false-colored)

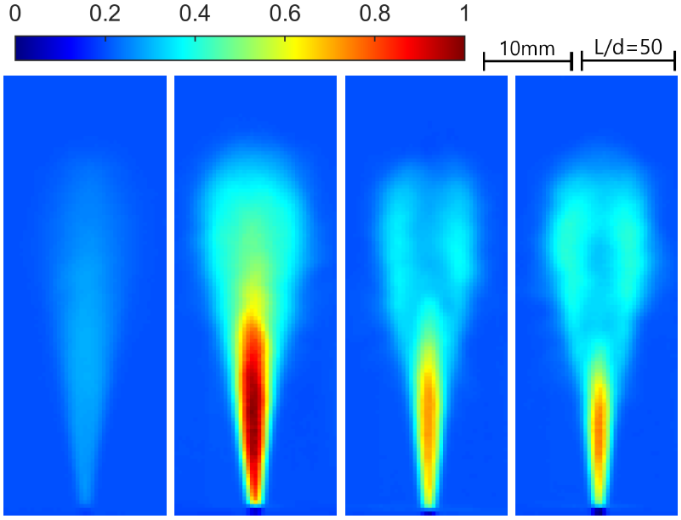

(a) Case 1 (b) Case 2 (c) Case 3 (d) Case 4

Fig. 6: Averaged IR images at 3 ms after start of injection (false-colored)

GALA e.V., Karlsruhe, Germany, ISBN 978-3-9816764-4-0

One potential reason is scattered IR radiation emitted from the chamber heaters installed at the top of the chamber, which maintain high-temperature environments near the sprays. The maximum ratio of scattering to absorption occurs when the wavelength of the incident ray is similar to the droplet diameter (Bohren und Huffman 2008). In contrast, the estimated Sauter-mean-diameters (SMDs) for all cases are approximately 16 µm, ignoring evaporation, which is five times larger than the filtered IR range (2.9 µm - 3.5 µm). Therefore, we can consider instead that the strong signal from the liquid core comes from IR absorption, however, different emissivity (Golzke et al. 2016). Focusing on downstream regions, Cases 1 and 2 have unimodal radial distributions for the IR signals, whereas Cases 3 and 4 have bimodal radial distributions, as shown in Figure 6. This is a unique observation in IR measurement, while the shadowgraphy and MS results show only unimodal shapes. The bimodal distribution denotes a strong emission at the boundary of the spray.

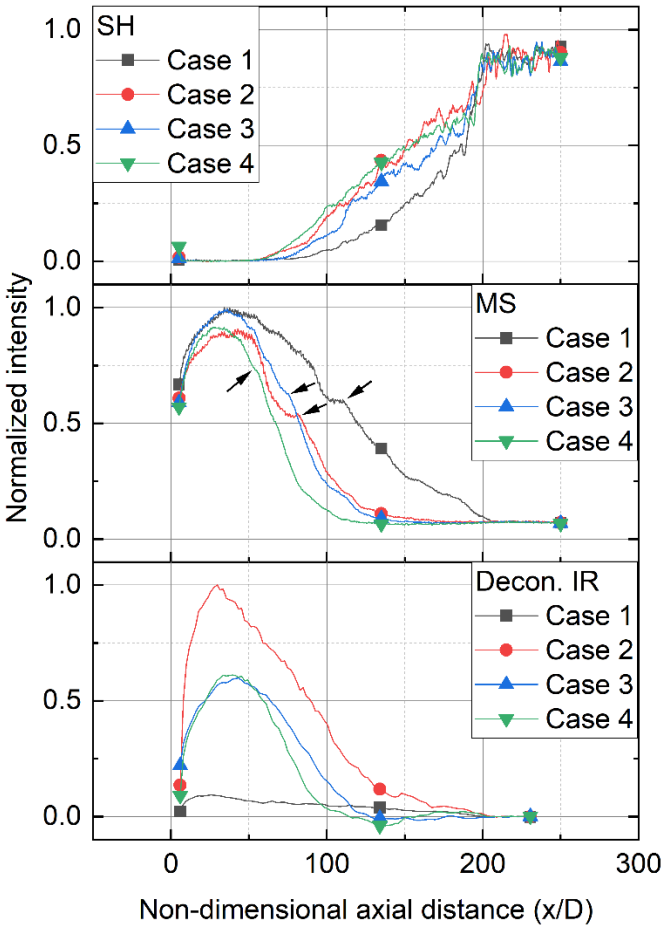

Fig. 7: Normalized axial distributions of spray images from shadowgraphy (SH), Mie-scattering (MS) and deconvoluted infrared radiation (Decon. IR)

The axial distributions of spray image intensities present a direct comparison as shown in Fig. 7. SH signals are fully extinct near the injector, where the MS signal is strong at the same region, indicating that the high density of the liquid spray blocks the background light. The SH intensities in other cases are overall brighter than in Case 1, implying that the sprays in Cases 2-4 are less dense due to the faster phase change caused by the higher chamber temperature. The axial distributions of the MS sprays reveal the phase change characteristics between subcritical and transcritical sprays. Cases 1 and 2 show distinct step-like transition points, as indicated by the arrows in Fig. 7, while Cases 3 and 4 show smoother transition. When the subcritical spray transitions to a supercritical fluid as transcritical phase change,

GALA e.V., Karlsruhe, Germany, ISBN 978-3-9816764-4-0

thermodynamic properties like density change smoothly rather than suddenly (Carlès 2010). This phenomenon is clearly observed by MS technique.
To clearly see the downstream regions of IR images, IR intensities are deconvoluted by using an inverse Abel transform (Cormack 1963), assuming an axisymmetric spray shape. The deconvoluted results represent cross-sectional IR radiation at different axial positions. Distinct negative signals are observed in Cases 3 and 4. Note that negative values do not indicate negative radiation. This means rather obstruction of background radiation, because the background-subtracted results were deconvoluted. This phenomenon implies a specific occurrence in transcritical sprays. The transcritical spray undergoes a phase change above the critical temperature as shown in Fig. 2. When the temperature approaches the critical point, critical opalescence can occur, causing high scattering effects and a milky appearance (Reamer und Sage 1957). Consequently, transmittance decreases during critical opalescence, with maximum opacity observed at the pseudocritical temperature (Xing et al. 2022). This results in blocking background signals by sprays, leading to negative values in the background-subtracted signals.

Conclusion

This study analyzed spray phase transition under sub- and transcritical conditions, relevant for high-pressure combustion devices. Using optical diagnostics such as shadowgraphy (SH), Mie scattering (MS), and infrared radiation (IR) measurements, cyclopentane sprays were investigated in a high-pressure, high-temperature spray chamber filled with gaseous nitrogen. Four cases were studied to compare spray characteristics under different injection conditions.

Results from SH and MS showed that the evaporation or supercritical phase changes occur earlier when the chamber temperature and the injection temperature increased. MS images revealed step-like transitions in the axial direction under subcritical conditions, indicating sudden fluid property changes from liquid to gas, which were not observed under transcritical conditions. Compared to SH and MS, IR images provided more information. The liquid core emitted a stronger signal in IR images, similar to MS; however, the background is blocked potentially due to different emissivity of the liquid phase compared to the gas phase. Additionally, IR images of transcritical sprays showed bimodal distributions potentially caused by critical opalescence, suggesting the presence of supercritical fluid.

The results from this study indicate that combining different optical diagnostic methods can provide a comprehensive understanding of spray characteristics. Further research is needed to clarify the interpretation of IR signals and better understand supercritical phases.

Acknowledgement

This research is funded by dtec.bw – Digitalization and Technology Research Center of the Bundeswehr under the project MaST - Macro/Micro-simulation of Phase Separation Phenomena in the Transcritical Regime. dtec.bw is funded by the European Union – NextGenerationEU. The authors thank the group Professur für Fluidsystemtechnik (FST), Friedrich-Alexander- Universität Erlangen-Nürnberg (FAU), and Telops Inc. for support of the experiments. Michael Pfitzner thanks ITIS e.V. for supporting his work.

GALA e.V., Karlsruhe, Germany, ISBN 978-3-9816764-4-0

References

Ahern, B., Djutrisno, I., Donahue, K., Haldeman, C., Hynek, S., Johnson, K., Valbert, J., Woods, M., Taylor, J., Tester, J., 2001: "Dramatic emissions reductions with a direct injection diesel engine burning supercritical fuel/water mixtures", SAE Transactions, pp. 1730-1735

Bell, I.H., Wronski, J., Quoilin, S., Lemort, V., 2014: "Pure and pseudo-pure fluid thermophysical property evaluation and the open-source thermophysical property library CoolProp", Industrial & Engineering Chemistry Research, 53, pp. 2498-2508

Bellan, J., 2020: "High-pressure flows for propulsion applications", American Institute of Aeronautics and Astronautics, Inc.

Bohren, C.F., Huffman, D.R., 2008: "Absorption and scattering of light by small particles", John Wiley & Sons

Carlès, P., 2010: "A brief review of the thermophysical properties of supercritical fluids", The Journal of Supercritical Fluids, 53, pp. 2-11

Chehroudi, B., Talley, D., Coy, E., 2002: "Visual characteristics and initial growth rates of round cryogenic jets at subcritical and supercritical pressures", Physics of Fluids, 14(2), pp. 850-861

Cormack, A.M., 1963: "Representation of a function by its line integrals, with some radiological applications", Journal of Applied Physics, 34(9), pp. 2722-2727

Golzke, H., Leick, P., Dreizler, A., 2016: "Differential infrared thermography of gasoline direct injection sprays", Quantitative InfraRed Thermography Journal, 13(1), pp. 50-69

JCGM, 2008: "JCGM 100: Evaluation of Measurement Data - Guide to the Expression of Uncertainty in Measurement", Joint Committee for Guides in Metrology

Lin, R., 2011: "Issues on clean diesel combustion technology using supercritical fluids: thermophysical properties and thermal stability of diesel fuel", Syracuse University

Liu, Y., Sun, X., Sethi, V., Nalianda, D., Li, Y., Wang, L., 2017: "Review of modern low emissions combustion technologies for aero gas turbine engines", Progress in Aerospace Sciences, 94, pp. 12-45

Ma, P.C., Bravo, L., Ihme, M., 2014: "Supercritical and transcritical real-fluid mixing in diesel engine applications", Proceedings of the Summer Program, Center for Turbulence Research, Stanford University, pp. 99-108

Neumann, P., Das Sharma, A., Viot, L., Trummler, T., Doehring, A., Son, M., Sander, T., Pfitzner, M., Zigan, L., Klein, M., Nitzke, I., Homes, S., Vrabec, J., Gratl, F., Newcome, S., Bungartz, H.-J., Stierle, R., Gross, J., Auweter, A., Tippmann, N., 2022: "MaST: Scale-Bridging Exploration of Transcritical Fluid Systems", dtec.bw-Beiträge der Helmut-Schmidt-Universität / Universität der Bundeswehr Hamburg, pp. 101-106, Universität der Bundeswehr Hamburg.

Reamer, H.H., Sage, B.H., 1957: "Demonstration of critical phenomena for pure substances and mixtures", American Journal of Physics, 25(2), pp. 58-63

Reitz, R.D., Bracco, F.V., 1986: "Mechanism of breakup of round liquid jets", Encyclopedia of Fluid Mechanics, 10, pp. 223-249

Riess, S., Weiss, L., Peter, A., Rezaei, J., Wensing, M., 2018: "Air entrainment and mixture distribution in Diesel sprays investigated by optical measurement techniques", International Journal of Engine Research, 19(1), pp. 120-133

Traxinger, C., Pfitzner, M., Baab, S., Lamanna, G., Weigand, B., 2019: "Experimental and numerical investigation of phase separation due to multicomponent mixing at high-pressure conditions", Physical Review Fluids, 4(7), 074303

Wensing, M., Vogel, T., Götz, G., 2016: "Transition of diesel spray to a supercritical state under engine conditions", International Journal of Engine Research, 17(1), pp. 108-119

Xing, K., Ji, Y., Wang, Z., Wang, M., Liu, Y., Xu, H., Xiao, G., 2022: "A potentially non-contact monitor method for CO2 at the pseudo-critical region using infrared spectrometer", Journal of CO2 Utilization, 56, 101842

GALA e.V., Karlsruhe, Germany, ISBN 978-3-9816764-4-0